Nuclear Science and Techniques **24** (2013) 040401

Geant4 simulation of plastic scintillators for a prototype μSR spectrometer

XU Wenzhen[1,2] LIU Yanfen[1,2] TAN Zongquan[1,2] XIAO Ran[1,2]
KONG Wei[1,2] YE Bangjiao[1,2,*]

[1]*State Key Laboratory of Particle Detection and Electronics, University of Science and Technology of China, Hefei 230026, China*

[2]*Department of Modern Physics, University of Science and Technology of China, Hefei 230026, China*

Abstract The experimental muon source on China Spallation Neutron Source (CSNS) is expected to be a high intensity (10^5 μ^+/s) surface muon source with a small beam spot of 4-cm diameter. For a practical application of this muon source, we are devoting to develop the first pulsed μSR spectrometer in China. In this paper, the performance of plastic scintillators in the μSR spectrometer is studied by Monte Carlo simulation. The processes such as positron energy deposition, scintillation photons production, light propagation and photon-electron conversion are carefully considered. According to the results, an optimal dimension of the plastic scintillator is proposed using for our future spectrometer, which has a long-strip shape with the dimension variation range of 50–60 mm length, 5–8 mm height, and 10–12 mm width. Finally, we can build a spectrometer with a count rate up to $10^4$$e^+$/s by 100–120 forward and backward segmental detectors in total. The simulation could serve as an important guide for spectrometer construction.

Key words μSR Spectrometer, Plastic scintillator, Monte Carlo simulation, Scintillation photon transmission

1 Introduction

China Spallation Neutron Source (CSNS) is an accelerator-based facility, including a proton accelerator, a neutron target station and multiplex neutron scatter spectrometers. An intensity neutron source will be produced by a 1.6-GeV proton beam bombarding a high Z metal target[1,2]. In the phase I, 120-kW proton beam, neutron beam intensity of 2.0×10^{16} n/cm^2·s, and 25-Hz synchronic frequency will be achieved. Besides serving as a neutron source, CSNS can also be used as a potential muon source[3]. The Experimental Muon Source (EMuS)[4,5], which is proposed for Phase I, is expected to perform a surface muon source with beam intensity of ~$10^5$$\mu^+$/s, beam spot of 4-cm diameter, and 1-Hz pulse frequency. Using this new muon source, a spectrometer for μSR spectroscopy (Muon Spin Rotation, Relaxation, Resonance, etc)[6,7] is essential to be developed now. Fig.1 schematically shows a pulsed μSR spectrometer. Nearly 100% polarized surface muons are injected into specimen and decay into positrons asymmetrically distributed in the full 4π solid angle. A muon counter before the μSR spectrometer is used to count incoming muons as a start-signal, and two sets of segmental detectors located forward and backward to the sample are used to detect the positrons as stop-signals. A lifetime of muons in materials could be measured by registering the start- and stop-signals. Finally, we could obtain the positron spatial distribution as time goes to explore the internal structure and dynamics in condensed matters under various extreme conditions.

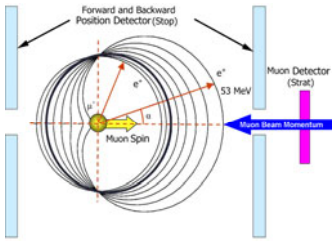

Fig.1 Schematic of the μSR detection system. Positrons from muon decay are asymmetrical distributed into space with an angular distribution: $P(\alpha)=1+A\cos(\alpha)$.

Supported by National Natural Science Foundation of China (No. 11075154).

* Corresponding author. *E-mail address*: bjye@ustc.edu.cn

Received date: 2012-09-18

Type of μSR spectrometer is dependent on the time structure of muon source: continuous or pulsed[8]. Benefiting from the development of detection and superconductor techniques, people are committing themselves to constructing some novel μSR spectrometers with improved performance. The photodiode detectors with small dimensions, high detection efficiency, and less magnetic sensitiveness are used to replace the traditional PMT in order to get higher resolution of 100 ps[9]. Superconductors are used to supply a high external magnetic field up to 5 T for the special μSR study[10]. Silicon microstrips are served as position-sensitive detectors for the study of spatial-temporal μSR spectroscopy[11]. New data acquisition systems are developed for vast scintillators detector system[12]. The realms of μSR spectroscopy will be dramatically broadened by these advanced techniques. For a pulsed μSR spectrometer construction, we have to utilize many small detectors in order to detect amounts of positrons in a short time interval of around 2.2 μs. The sizes of scintillator detector play a significant role in structure designing, optical coupling, light transmission and signal processing etc. Unfortunately, the performance of the positron detectors are impossibly conducted using a variable energy positron beam of 0–53 MeV, one only decide the scintillator parameters by experience. So, we performed some Monte Carlo simulation to study the plastic scintillator in the μSR detector system, and other simulations for μSR spectrometer construction could be found in Refs. [13,14].

In Section 2, the simulation configuration, parameters and approaches are briefly introduced. Many physical quantities are studied, such as the energy deposition and the muons energy loss rate (K) in a scintillator, the transition probability (P) of positron energy to scintillation photons, light yield (R) and the light transmission efficiency (T) in some mediums. The simulation results were analyzed and discussed in Section 4. Finally, a preliminary proposal for our future spectrometer construction is given based on our simulation.

2 Simulation, configuration and methods

The physical process is to be simulated as follows: the high intensity surface muons up to $10^5\mu^+$/s are injected into specimen, stopped and decayed into positrons, the positrons are detected by transporting and collecting the scintillation photons produced by the ionization loss of energy in scintillators. In this process, the electromagnetic interactions among particles and materials and optical processes can be simulated by a Monte Carlo code — Geant4[15,16]. This tool allows us to set many flexible and modular simulation conditions, such as the detector dimensions, the reflector configuration used for scintillator wrapping, the properties of optical mediums with an optical coupling and the realistic scenario of PMT response. Fig.2(a) shows a single channel for positron detection by a plastic scintillator in the μSR spectrometer system. Simulation was carried out using the long-strip EJ-200 plastic scintillators with dimensions of 30–100 mm length, 5–15 mm height and 5–15 mm width. The main characteristics of the scintillator are summarized in Table 1(a). Length (L) and width (W) will determine the count rate of the single-channel detector or the integral spectrometer. Meanwhile, light transmission efficiency and positron energy deposition are evidently dependent on length (L) and height (H). In our simulation, the photon exit surface of the scintillator $H\times W$ is connected with a light guide end of 5 mm×5 mm using the silicone optical grease of 1.5-refractivity, while the other surfaces are covered with a Teflon reflective coating. A 1-meter-long clear fiber BCF-98 served as light guide is used to connect the scintillator to transport the scintillation light to a PMT (ET 9813B (Table 1b). Detection and measurement can be free from the high magnetic filed of several thousands Gauss in the central area of spectrometer. This clear light guide, which has double claddings of 0.5 mm thick Acrylic inner and 0.1 mm thick Fluor-Acrylic outer, is reported in Table 1(c). The maximum incidence angle of the total- reflection light in the fiber, which can be defined as ϕ_{max} with respect to the long axis of the fiber, is given by $\sin\phi_{max}\sqrt{[(n_1^2-n_3^2)/n_0^2]}$, where, n_1 and n_3 are the refractive of the core material and the outer cladding of the fiber. n_0 is the refractive of the silicon grease coupled with the fiber ends. The ϕ_{max} around 30 degree calculated by the parameter values can be obtained. Therefore, a fraction of photons exiting out the scintillator will be inevitably lost at the front end of light guide. The last part of our

simulation in Fig.2(a) is the photon-electron conversion by modeling the PMT cathode realistically, including a 5 mm thick, 51 mm diameter quartz window connected with the exit end of light guide and blue-green sensitive bialkai photocathode.

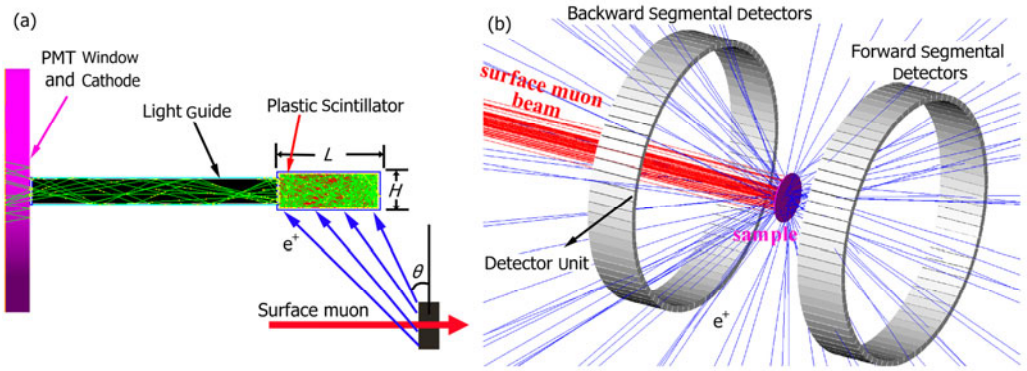

Fig.2 (a) Sketch to illustrate the principle used for positron detection by plastic scintillator. Positrons from muon decay inject into the scintillator strip at an incident angle θ with respect to the normal of the incident surface. (b) 3D view of segmental detectors in μSR spectrometer.

Table 1 Tables with detector properties used in simulation

(a) EJ-200 scintillator			
Base			Polyvinyltoluene
Atomic ratio (H:C)			11:10
Density (g cm^{-3})			1.023
Refractive index			1.58
Light output (% anthracene)			64
Scintillation yield (photons/MeV)			10,000
Emission peak (nm)			425
Decay time (ns)			2.1
(b) ET 9813B			
Refractive index			1.49
Effective photocathode diameter(mm)			46
QE peak (%)			30
Gain			70×10^6
Rise time (ns)			2
Transit time(ns)			46
(c) BCF-98			
	Material	Refractive index	Numerical aperture
Core	Polystyrene	n_1=1.60	/
Cladding 1	Acrylic	n_2=1.49	0.58
Cladding 2	Fluor-acrylic	n_3=1.42	0.74

For realistically treating the interactions of the scintillation photons with dielectric surfaces, two optical reflection models—the glisur model and the unified model[17] were carefully set in our simulation. The surface type was dielectric_dielectric photodiodes for the Teflon reflector, where the unified model was used with the reflection type set to 100% specular lobe distribution. For all grease-coupled surfaces, dielectric_dielectric was set as surface type with the glisur model so as to use the Fresnel formulas for optics calculation. The surface finish was set to ground back painted (Sigma Alpha=0.2)[18] and polished for the unified and the glisur model. To keep the scintillator and the light guide away from the outside light exposure, the dielectric_metal with the glisur model (reflectivity: 0, quantum efficiency: 100%) is defined as a photon absorber attached to the outermost layer. In order to directly count the photoelectrons converted by the coming scintillation photons, dielectric_metal with the glisur model (reflectivity: 0.2, quantum efficiency: 30%) is defined as a PMT cathode attached behind the quartz window.

To estimate the positron count rate of a single detector or the spectrometer, we studied a traditional spectrometer including two symmetrical detector segmentations forward and backward (Fig.2b). The inner end surface ($H\times W$) of either segmental detectors ring are 7.5 cm away from the sample center, and the detector unit is 10 cm far from the ring center so as to save moderate space to match a compromise for enough sample chamber space and sufficient detection solid angle.

3 Results

Firstly, the positron deposited energy in the scintillators with variable dimensions was studied by perpendicularly injecting positron into the down surface and counting the exit positrons from the upper surface. The deposited energy can be calculated by subtracting the exit energy from the coming energy. The scintillators in this simulation have a fixed length of 40 mm and width of 10 mm, but variable height of 5–16 mm. Fig.3(a) shows the deposited energy as a function of positron incident energy of 0–53 MeV for different scintillator heights. Fig.3(b) shows the energy loss ratio as a function of positron incident energy for variable scintillator heights. An empirical equation for energy loss ratio (K) depended on incident energy (E) and penetration height (H) can be obtained.

$$K(E,H)=(0.12e^{-E/6.3}+0.017)+(0.084e^{-E/55}+0.0072)H \quad (1)$$

Where E is the range of 5 to 53 MeV, H is penetration distance (mm). The constant coefficients for Eq.(1) are calculated by linear fitting (R^2>0.98) and two single-exponential curves fitting (Chi^2/DoF≈0) based on the data (Fig.3b).

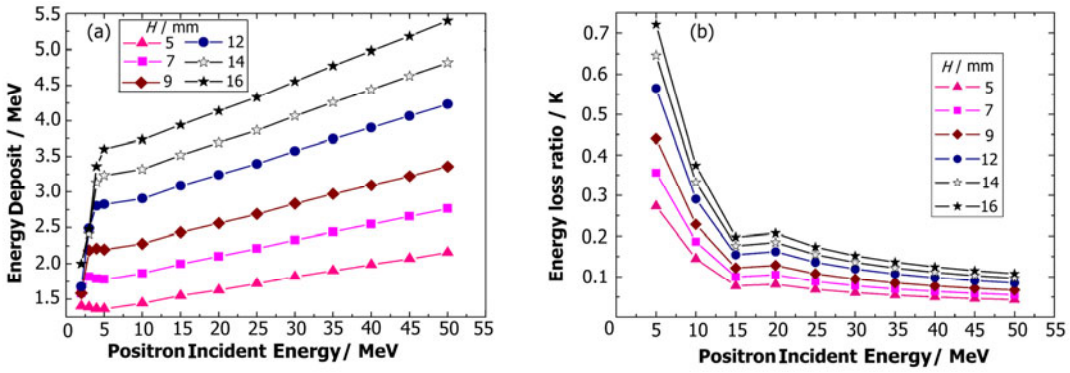

Fig.3 (a) Deposited energy as a function of positron incident energy for nine different height scintillators; (b) Energy loss ratio as a function of positron incident energy for variable scintillator height.

Figure 4 shows that the light yield of positrons in the scintillator was calculated with the same sizes as the previous deposited energy simulation at variable height of 5–16 mm. The vertical axis means the total light yield of one parametered scintillator as a function of positron energy of 0–53 MeV. The filled dots (a, b, c and d) mean the maximum light yield at some certain energy for different scintillator heights. Comparatively, the dot O is marked as the light yield of 0.511 MeV γ-rays in the scintillator. As mentioned in Section 2, the scintillation photons are transported far from the sample room via a long light guide, avoiding the high magnetic field influence. Consequently, a considerable light loss dependent on the scintillator sizes and light guide is expected at the beginning of light guide.

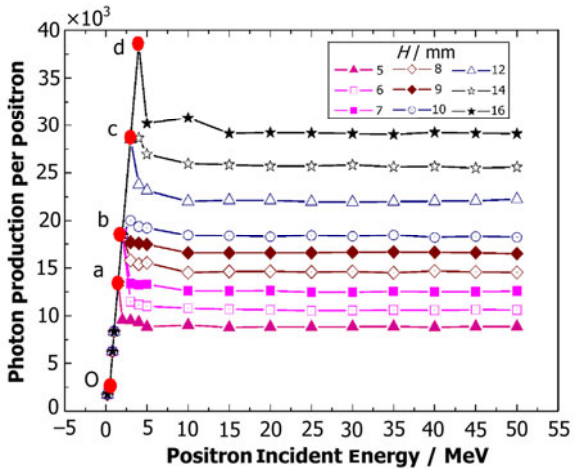

Fig.4 Scintillation photon yield for variable scintillator under different incident energy. The red filled dots a, b, c and d indicate the approximate maximum photon production for the variable scintillator heights. Dot "O" means the photon production for the 0.511-MeV gamma rays.

In our case, the loss is up to 40% when setting an exit scintillator surface of 5 mm×10 mm (H×W) and an entry light guide surface of 5 mm×5 mm. For realistically studying, the positrons are to be injected into scintillators with a variable incidence angle (θ) (Fig.2a). On the other hand, the length of the scintillator strip determines the θ range in our simulation. For example, a 50-mm-long scintillator strip means that θ range of 38 degree to 50 degree was calculated according to the spectrometer configuration. Fig.5 shows the photoelectron count as a function of θ incident angle for six different lengths. The solid lines are linear fitting for these data.

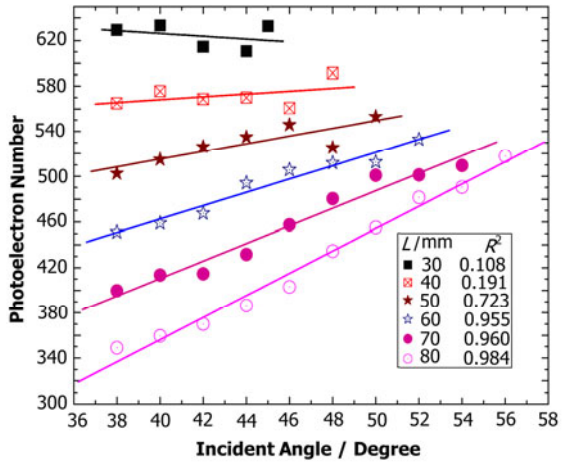

Fig.5 Photoelectron yield as a function of e^+ incident angle for different scintillator lengths. The lines indicate the linear fit for the different lengths. The correlation coefficient R^2 in the legend represents the goodness of linear fit, which is in range from 0 to 1.

The expected pulsed width of surface muon beam at EMuS is about 100 ns smaller than the 2.2-μs muon lifetime. We have to detect the majority of positrons from muon decay in 2.2 μs after the muon beam reaching the specimen. When defining the Minimum Detection Time per Event (MDTE), the detection time for a single event in a detector unit should not be less than the ratio of one 2.2-μs muon lifetime to the total counts of positrons hitting on a single scintillator strip. A small MDTE is important for us to avoid data piling up. Fig.6 shows that the MDTE for the different length and width of scintillators in simulation had an intensive surface muon beam of $10^5\mu^+$/s. Selecting the crystals with different width (8, 10, 12, 20 mm) represents the detector ring with different segmental counters to be configured. For example, an 8-mm-width plastic scintillator used as detector unit means 78×2 segmentation counters capably integrated in our spectrometer. The other width size can be detailed in the inset. Additionally, the scintillator length is from 30 mm to 70 mm.

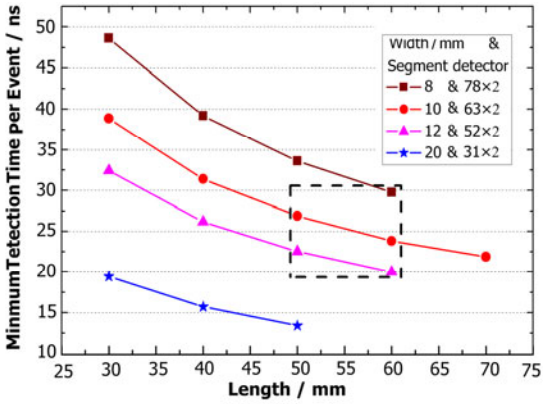

Fig.6 Minimum detection time per event for different dimensions of scintillators. The dashed box means that the parameter option in this area meets the requirements of our optimal design.

4 Discussion

For a given height scintillator, we can find that deposited energy increases with the incidence energy of positrons (Fig.3a), whereas the energy loss ratio $K(E)$ indicates an exponentional reduction (Fig.3b). But in the case of injecting a given energy positron, the longer path positron experience (H) is, the more energy deposited in scintillator is. And the function $K(H)$ approximately behaves as a linear increase. Additionally, it is not a linear relation between the light yield and the incidence energy (Fig.4). For the scintillator height of 5 mm to 16 mm, we define the positrons with energy of less than 5 MeV as Low Energy Positron (LEP). The LEP can be completely stopped in the scintillator, resulting in a light yield in proportion to incident energy. Further, the stopped positrons will be annihilated with electrons, yielding two 0.511 MeV gamma rays. Illumining the scintillator by these gamma rays will add light yield to our calculation. The filled dots (a, b, c, and d in Fig.4) give an evidence that the 0.511 MeV gamma rays do produce many additional photons. However, for positron energy of larger than 5 MeV so-called Medium Energy Positron (MEP), the light yield is not linearly increasing with incident energy. This is mainly due to the limited scintillation light yield in a fixed-

length scintillator for the Minimum Ionizing Particles (MIP). Consequently, its light yield R in a given scintillator is only dependent on the height size (H mm): $R(H) = -442 + 1880H$. Finally, the effective efficiency of the energy-light conversion can be obtained by Eq.(2).

$$P = \frac{Rh\bar{\nu}}{EK} = \frac{(-442+1880H)h\bar{\nu}}{\left[(0.12e^{-E/6.3}+0.017)+(0.084e^{-E/5.5}+0.0072)H\right]E} \quad (2)$$

where, E is in the range of 5 to 53 MeV.

It is concluded that the decreasing energy loss ratio and conversion efficiency, which are opposite to the increasing deposited energy, exactly ensure the output electronic signals with close amplitudes for different position incidence energy. With this result, we can easily distinguish the MEP and background particles in detection, and realize positrons detection with nearly full energy spectrum and indiscrimination for energy range of 5 to 53 MeV. Avoiding the undesired LEP positron detection, a thin aluminium layer is usually placed before the scintillator[19]. According to the light yield in scintillators with height 5 mm, the light yield count is large enough up to 10^4, for us to distinguish the background of a 0.511-MeV light yield (for comparison in Fig.4 filled dot O). In consideration of scintillator-guide coupling and the cost of light guide, we selected the 5-mm height scintillator for our simulation and future experiments.

The distance (D) between the incident position of positrons and the light-exit surface of the scintillator significantly determinates the light transmission efficiency. An optimal length of the scintillator strip has to be found for our spectrometer design. Generally speaking, there is a liner relation between photons loss in the strip and the D. Especially for strip of larger than 60-mm length, the values of R^2 are close to 1 (Fig.5), meaning that the photon loss in scintillator is well linear with the D. The large length of the scintillator strip is the main reason of the photon loss. For 80-mm length scintillator, the efficiency of photon collection for the positrons with θ=38° (positrons hitting on the right end of scintillator in Fig.2a) is only ~60% for θ = 56°(light-exit end). In this case, the final electronic signal amplitudes will be so evidently different that it is difficult for discrimination threshold setting. However, for the length 30 mm and 40 mm, it is found that the photon collections for different incident angles are not marked different but fluctuant. There is no clear regularity for the photon counts at different incident angles. The very small R^2 (< 0.2) clarifies the slight relation between length and photon loss. The fluctuation of photon count may be mainly due to the different incident angle, statistical fluctuation or some optical physics processes. Consequently, the scintillator strip with length 30–60 mm is suitable for us to control the signal difference of less than 20%. In this case, we can obtain an average photoelectron count up to 500 electrons per event, resulting in a voltage output up to ~1 V after the photoelectrons multiplier by PMT (gain 10^6, load resistance 50 Ω). However, a determinate length scintillator must be associated with the detection rate which is strongly dependent on length and width. From Fig.6, the selecting a scintillator strip with larger width and length requires a higher detection rate of single detection channel or integral spectrometer. The detection time per event can be achieved in a low value about 20–30 ns for the traditional detection equipments, including the fall time in scintillator, transmission time, the rising time in PMT and the pulsed width necessary for electronic system in total. With a comprehensive consideration, the scintillator with 50–60 mm length and 10–12 mm width is optimal for the positron detection in our μSR spectrometer design (Black dashed box in Fig.6 shows this optimal result). Finally, we can obtain a desired performance of our future spectrometer based on the design in this paper: The 100–120 detection channels can be sufficiently segmented on the forward and backward detector rings, the detection rate can be up to 70–90 e^+/s and ~1.0×10^4 e^+/s for a single detection unit and whole spectrometer, respectively. The performances meet the requirements of the μSR.

5 Conclusion

We have used Geant4 code to study the electromagnetic processes and the optical processes in

muon lifetime detection, and investigated the suitable setup and the expected performance of the μSR spectrometer at CSNS EMuS. The significant parameters as deposited energy, light yield, energy-light conversion efficiency and transport efficiency were calculated and studied, supporting that the scintillator sizes play an important role in μSR spectrometer construction. A plastic scintillator strip with 50–60 mm length, 10–12 mm width, and 5 mm height was testified as an optimal positron detector for our μSR spectrometer. The high light yield and the light transmission efficiency in this scintillator meet the requirements for signal discrimination and μSR spectroscopy measurement. At present, a μSR spectrometer with 100–120 segmental detection channels is under design and construction at EMuS. The experimental studies of plastic scintillators, a single detection channel, a multi-channels spectrometer system and the data acquisition (DAQ) system are in progress.

Acknowledgements

We thank Prof. Jingyu Tang and Dr. Hantao Jing for useful discussion about the muon source and μSR spectrometer construction at China.

References

1 Wei J, Chen H S, Chen Y W, *et al*. Nucl Instrum Meth A, 2009, **600:** 10–13.

2 Liu R H, Zhang J S, Qu H M, *et al*. Nucl Sci Tech, 2012, **23:** 328–331.

3 Tang J Y, Fu S N, Jing H T, *et al*. Chin Phys C, 2010, **34:** 121–125.

4 Jing H T, Meng C, Tang J Y, *et al*. Nucl Instrum Meth A, 2012, **684:** 109–116.

5 Xu W Z, Liu Y F, Ye B J. Plasma Sci Technol, 2012, **14:** 469–472.

6 Cox S F J. J Phys C: Solid State Phys, 1987, **20:** 3187–3319.

7 Yaouanc A, Dalmas de Réotier P. Muon spin rotation, relaxation and resonance: Applications to condensed matter, Oxford: Oxford University Press, 2011.

8 Nagamine K. Introductory Muon Science, Cambridge: Cambridge University Press, 2003, 115–120.

9 Stoykov A, Scheuermann R, Sedlak K, *et al*. Nucl Instrum Meth A, 2009, **610:** 374–377.

10 Salman Z, Baker P J, Blundell S J, *et al*. Phys B, 2009, **404:** 978–981.

11 Shiroka T, Renzi R De, Bucci C, *et al*. Phys B, 2006, **374/375:** 494–497.

12 Chen Y, Zhang Z M, Li D W, *et al*. Nucl Sci Tech, 2012, **23:** 144–149.

13 Sedlak K, Scheuermann R, Stoykov A, *et al*. Phys B, 2009, **404:** 970–973.

14 Sedlak K, T Shiroka, Stoykov A, *et al*. IEEE Nucl Sci, 2010, **57:** 2187–2195.

15 Agostinelli S, Allison J, Amako K, *et al*. Nucl Instrum Meth A, 2003, **506:** 250–303.

16 Su J, Wang H X, Xue Q, *et al*. Nucl Tech, 2011, **34:** 575–580. (in Chinese)

17 Levin A, Moisan C. IEEE Nucl Sci Symp Conf Rec, 1996, **2:** 702–707.

18 Janecek M, Moses W W. IEEE Nucl Sci, 2010, **57:** 964–970.

19 Tanaka H K M, Nagamine K, Miyadera H, *et al*. Nucl Instrum Meth A, 2005, **554:** 201–211.